LETTERS

Direct observation of the mechanochemical coupling in myosin Va during processive movement

Takeshi Sakamoto[1], Martin R. Webb[2], Eva Forgacs[3], Howard D. White[3] & James R. Sellers[1]

Myosin Va transports intracellular cargoes along actin filaments in cells[1]. This processive, two-headed motor takes multiple 36-nm steps in which the two heads swing forward alternately towards the barbed end of actin driven by ATP hydrolysis[2]. The ability of myosin Va to move processively is a function of its long lever arm, the high duty ratio of its kinetic cycle and the gating of the kinetics between the two heads such that ADP release from the lead head is greatly retarded[3–10]. Mechanical studies at the multiple- and the single-molecule level suggest that there is tight coupling (that is, one ATP is hydrolysed per power stroke), but this has not been directly demonstrated[4,5,11]. We therefore investigated the coordination between the ATPase mechanism of the two heads of myosin Va and directly visualized the binding and dissociation of single fluorescently labelled nucleotide molecules, while simultaneously observing the stepping motion of the fluorescently labelled myosin Va as it moved along an actin filament. Here we show that preferential ADP dissociation from the trail head of mouse myosin Va is followed by ATP binding and a synchronous 36-nm step. Even at low ATP concentrations, the myosin Va molecule retained at least one nucleotide (ADP in the lead head position) when moving. Thus, we directly demonstrate tight coupling between myosin Va movement and the binding and dissociation of nucleotide by simultaneously imaging with near nanometre precision.

The ability to visualize the binding of fluorescent nucleotides to myosin in the light microscope has been limited by technical problems, such as the nonspecific binding of the fluorescent nucleotide to the coverslip, low quantum yield and rapid photobleaching. This has limited the maximum nucleotide concentration that could be used with analogues such as Cy3-labelled ATP to less than 100 nM[12–15]. To overcome these problems, we have used a fluorescent ATP analogue (3′-(7-diethylaminocoumarin-3-carbonylamino)-3′-deoxyadenosine-5′-triphosphate; deac-aminoATP), in which the fluorescence emission increases ~25-fold (Supplementary Fig. 1) when bound to a heavy meromyosin-like fragment of myosin Va (MyoV-HMM) in solution[16,17]. The kinetic mechanism of MyoV-HMM using deac-aminoATP as a substrate has been thoroughly studied, including the extent of gating that occurs between the two heads during movement[10,17]. In brief, deac-aminoATP binds 3-fold faster to MyoV than ATP does, and deac-aminoADP dissociates 10–20-fold slower than ADP[17]. When MyoV-HMM is bound to actin by both heads, the release rate of deac-aminoADP from the lead head is decreased by about 30-fold compared to the unstrained rate[10]. The processive run length of MyoV-HMM on actin using deac-aminoATP as a substrate is shorter (1,050 ± 80 nm) than when using ATP alone (1,950 ± 160 nm) (Supplementary Figure 2a). The maximal velocity of movement on actin at saturating deac-aminoATP is 120 nm s^{-1}, approximately 8–10-fold less than observed with ATP[10] (Supplementary Fig. 2b).

Deac-aminoADP that was non-specifically bound to a coverslip surface in the absence of MyoV-HMM was visualized using an electron multiplying charged coupled device (EMCCD) camera at a camera gain level of 1,000 (the scale for gain is 0–1,000; Fig. 1a, e). The gain on the camera chip was then reduced to 400, at which the intensity of the nonspecifically bound deac-aminoADP spots was considerably reduced (Fig. 1b, f). However, at the same gain (400) and collection time of 330 ms, deac-aminoADP that was bound to MyoV-HMM on the coverslip (Fig. 1c, g) had a sufficiently high intensity (>10,000 photons) to fit the point-spread function of a single spot and so determine its precise nanometre localization[18] (Supplementary Fig. 3). At the single-molecule level, we found a 4-fold enhancement of the fluorescent intensity of deac-aminoADP on binding to MyoV-HMM.

We exchanged Alexa-Fluor-568-labelled calmodulins for the endogenous calmodulin bound to the neck region of MyoV-HMM. On average, each calmodulin contained 1.8 Alexa Fluor 568 moieties, and three Alexa-Fluor-568-labelled calmodulins were exchanged per MyoV-HMM, making it much brighter than myosin fused to GFP molecules or containing a single Cy3- or rhodamine-labelled calmodulin that had been previously used for single-molecule studies[3,18]. Similar estimates for labelling ratios were obtained by using spectrophotometric techniques in solution or by examining the photobleaching kinetics of the molecules in the microscope (Supplementary Fig. 4). This allowed the Alexa-Fluor-568–MyoV-HMM to be as bright as the deac-aminonucleotides, and permitted the same camera and camera settings to be used to image both (Fig. 1d, h and Supplementary Fig. 3).

We simultaneously visualized Alexa-Fluor-568–MyoV-HMM and deac-aminonucleotide during processive movement on actin filaments *in vitro* (Fig. 2a, b; Supplementary Fig. 5 and Supplementary Movie). The Alexa-Fluor-568–MyoV-HMM and the deac-aminonucleotide fluorescence moved in the same direction at the same rate and on the same actin filaments (Fig. 2a, b and Supplementary Figs 5 and 6). The fluorescent signal from Alexa-Fluor-568–MyoV-HMM moved in 36-nm steps as would be expected from a molecule, in which both heads were labelled (Fig. 2a), albeit there is the possibility of minor differences between the alternating step sizes due to unevenness in the labelling of the two heads (see Supplementary Fig. 7 for an example of 'limping' movement). The deac-aminonucleotide moved in 18-nm steps. One step occurred simultaneously with the MyoV-HMM step, whereas the other step occurred during a dwell in the MyoV-HMM movement (Fig. 2b). These observations from a single trace are reinforced by examining histograms of the MyoV-HMM step size (which shows a peak of 36 ± 7 nm; Fig. 2d) and of the deac-aminonucleotide step size (which shows two peaks of 18 ± 7 nm and 36 ± 9 nm; Fig. 2e). The larger, 36 nm values for the deac-aminonucleotide movement are expected to result when two 18-nm movements occurred without a discernable dwell between them. This is calculated to occur 22–37% of the time ($1\text{-}e^{-kt}$) on the basis of the deac-aminonucleotide association

[1]Laboratory of Molecular Physiology, National Heart, Lung and Blood Institute, Bethesda, Maryland 20892, USA. [2]MRC National Institute for Medical Research, Mill Hill, London NW7 1AA, UK. [3]Department of Physiological Sciences, Eastern Virginia Medical School, Norfolk, Virginia 23507, USA.

and dissociation rate constants measured in Fig. 3 and the 330 ms data acquisition time. The intensity of the deac-aminonucleotide signal integrated from a 12 × 12 pixel (840 × 840 nm^2) area surrounding the molecule at each frame showed a bimodal distribution in which one peak contained a factor of two more photons per frame than the other (Supplementary Fig. 8). The photon count in the smaller peak represents one deac-aminonucleotide per MyoV-HMM, whereas that in the other represents two per MyoV-HMM. Note that this nucleotide has similar fluorescence intensity when bound as MyoV-HMM-ADP, MyoV-HMM-ADP-P_i or MyoV-HMM-ATP, and thus, we cannot discriminate between different nucleotide states of a single head by intensity[17]. Using this criterion, the normalized intensity of the deac-aminonucleotide signal was also plotted as a function of time (Fig. 2c) and was shown to change from a value of one to two during each MyoV-HMM step and then decrease from a value of two to one during the MyoV-HMM dwell period.

The model to account for the 36-nm Alexa-Fluor-568–MyoV-HMM steps and the 18-nm deac-aminonucleotide steps is shown in Fig. 2f. Initially, MyoV-HMM has deac-aminoADP bound to both heads and the position of the Alexa-Fluor-568–MyoV-HMM and the deac-aminonucleotide spots are coincident (step 1). Deac-aminoADP is then released from the trail head, which results in the position of the deac-aminonucleotide signal advancing by 18 nm

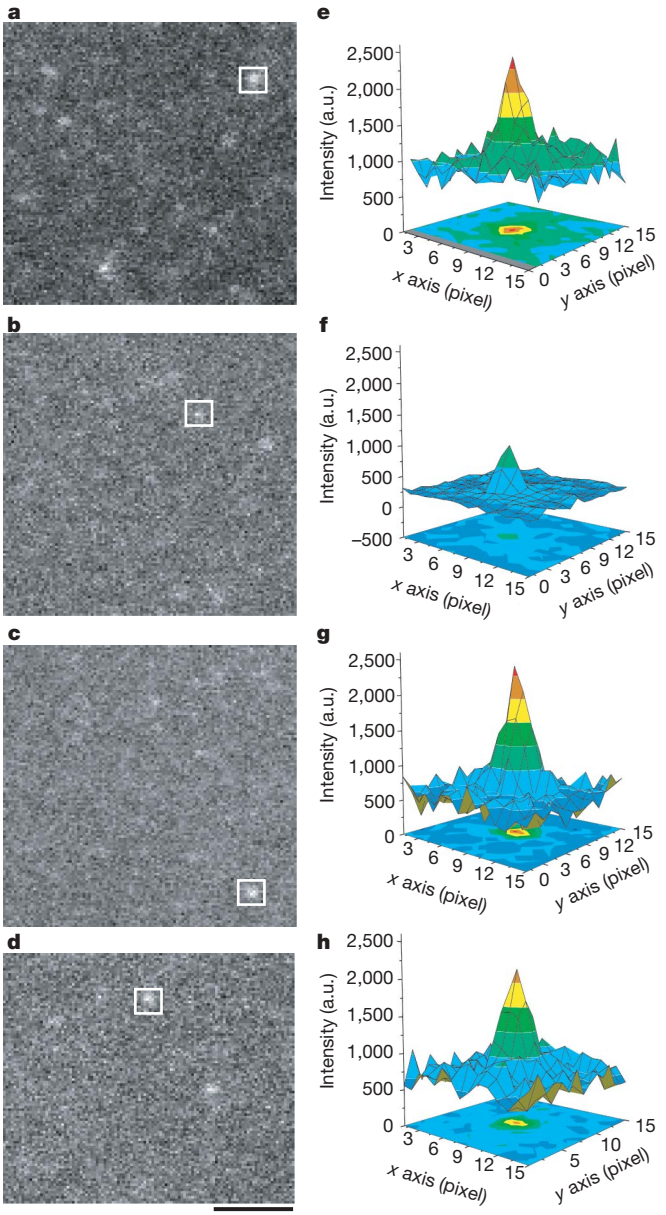

Figure 1 | Imaging deac-aminoADP and Alexa-Fluor-568–MyoV-HMM. **a**–**d**, TIRF-microscopic images (110 × 100 pixels) are shown. Deac-aminoADP was imaged at 442 nm (**a**–**c**); Alexa-Fluor-568–MyoV-HMM was imaged at 568 nm (**d**). Two-dimensional intensity profiles from each white square in **a**–**d** are shown in **e**–**h**. **a**, **e**, Deac-aminoADP bound directly on the coverslip, with maximal camera gain (1,000). **b**, **f**, Deac-aminoADP bound directly on the coverslip surface at a camera gain of 400. **c**, **g**, Deac-aminoADP bound to MyoV-HMM at a camera gain of 400. **d**, **h**, Alexa-Fluor-568–MyoV-HMM bound to the surface at a camera gain of 400. All data were taken with an iXon+ camera (DV897, Andor technology) at 10 MHz readout at a constant laser power. The background level was fixed at about 750 (arbitrary units, a.u.) intensity. Scale bar, 2 μm

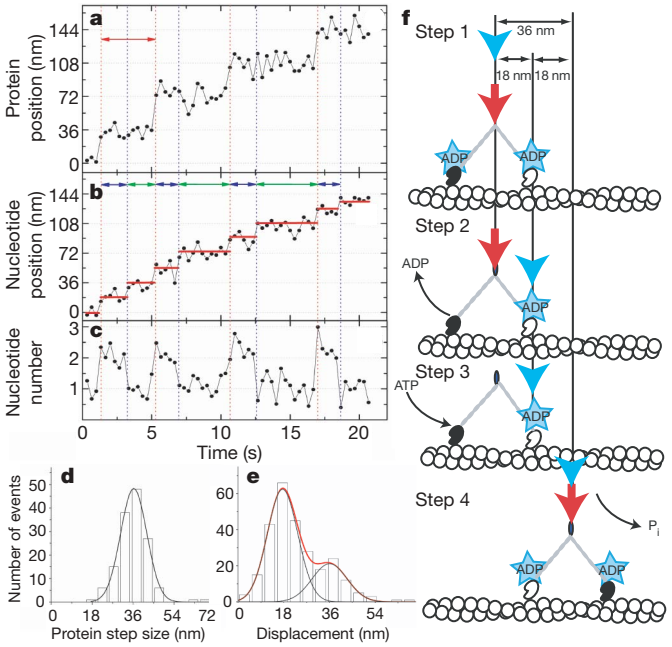

Figure 2 | Correlation between the movement of MyoV-HMM and the binding/dissociation of deac-aminonucleotide. Images of Alexa-Fluor-568–MyoV-HMM and deac-aminoATP fluorescence were acquired simultaneously with a Dual-View system. The excitation/emission wavelengths of Alexa Fluor 568 are distinct from those of deac-aminoATP, allowing simultaneous visualization of the MyoV-HMM and the nucleotide. The photons from the spots were acquired using 330 ms integrations and the point spread function from each spot was fit with a two-dimensional Gaussian to determine the location of the fluorophor(es) at each time point[18]. The deac-aminoATP concentration was 200 nM. **a**, The protein fluorescence data show ~36-nm steps, which are marked by red vertical dotted lines. Red double-ended arrows delineate the dwell time of a step. **b**, The deac-aminonucleotide stepping events are marked by alternating red and blue vertical dotted lines. Red vertical dotted lines are steps of both MyoV-HMM and deac-aminonucleotide, whereas blue vertical dotted lines show only stepping of deac-aminonucleotide. Individual spots move in a stepwise manner in the same direction as the MyoV-HMM. Dwell times are marked by blue and green double arrows. Red horizontal lines mark the average position of the spot during a pause. **c**, Normalized intensity of the deac-aminonucleotide fluorescence. **d**, Step-size histogram for the movement of Alexa-Fluor-568–MyoV-HMM (n = 145 steps, 38 MyoV-HMM molecules). The curve represents the fit to a Gaussian distribution (mean ± s.d., 36.3 ± 7.2 nm.) **e**, Step-size histogram for the movement of the deac-aminonucleotide (n = 267 steps, 38 MyoV-HMM molecules). The red curve represents the fit to the sum of two Gaussians (shown individually in black lines; mean ± s.d., 17.5 ± 7.1 nm, 36.0 ± 8.6 nm). **f**, Model for correlation of movement of Alexa-Fluor-568–MyoV-HMM and deac-aminonucleotide binding and dissociation. The red and blue arrows show the position of the centroid of the Alexa-Fluor-568–MyoV-HMM and of the deac-aminonucleotide fluorescence, respectively. See text for description of the model; see also Methods.

(step 2). After deac-aminoATP binds to the nucleotide-free trailing head, this head rapidly dissociates and swings forward to rebind and become the new lead head (steps 3 and 4). Single-molecule and bulk solution studies suggest that the time between detachment of the trailing head, followed by its forward swing and reattachment, is a few milliseconds and is thus much faster than the sampling rate (330 ms) used in our experiments[7,10,11,19]. Therefore, ATP binding to the trail head, dissociation of that head, and stepping and rebinding are all associated with a 36-nm movement of the MyoV-HMM molecule and a simultaneous 18-nm movement of the deac-aminonucleotide signal. The binding of deac-aminoATP to the trail head might be expected to produce a transient backward movement of the nucleotide fluorescence centroid, but this is not seen because the trail head quickly detaches and is rapidly moved forward by the power stroke occurring on the lead head.

To confirm the model, lifetimes during the two and one deac-aminonucleotide signal levels were analysed at three different deac-aminoATP concentrations (Fig. 3). We interpret the two to one nucleotide signal decrease to be associated with deac-aminoADP release from the trail head, whereas the one to two nucleotide signal increase is associated with deac-aminoATP binding to that head. Thus, fitting the lifetimes of the high nucleotide signal at 100, 200 and 400 nM deac-aminoATP showed no statistical difference in the rate of deac-aminoADP dissociation (0.82 s^{-1}, 0.79 s^{-1} and 0.90 s^{-1}, respectively; Fig. 3a–c). This is similar to the deac-aminoADP dissociation rate constants measured in solution under identical conditions using stopped-flow spectrofluorimetry (1.2 s^{-1}; Supplementary Fig. 9c). This would indicate that in our experiments there is no acceleration of the deac-aminoADP release from the trail head and is consistent with stopped-flow kinetic results previously reported[10]. An acceleration of the ADP release rate from a positively strained trail head of up to 50-fold was previously predicted if the lead head were to complete its power stroke when both heads were attached[9]. However, an earlier study found that the lead heads were only at the start of their power stroke[20], which is consistent with the lack of acceleration of ADP release from the rear head observed in our study. On the other hand, the observed deac-aminoATP binding rates determined by fitting the lifetimes of the low signal level intermediate increased as the deac-aminoATP concentration used was raised from 100 to 200 to 400 nM (0.53 s^{-1}, 0.64 s^{-1} and 1.02 s^{-1}, respectively; Fig. 3d–f). This corresponds to a second order association rate constant of 1.67 $\mu M^{-1} s^{-1}$, which is very similar to a value of 2.48 $\mu M^{-1} s^{-1}$ measured in solution under identical conditions (Supplementary Fig. 9b).

These results support a model in which the trailing head of the MyoV-HMM molecule releases ADP much more rapidly than the leading head[2,9,10]. In fact, solution kinetics studies at 20 °C demonstrated that the deac-aminoADP dissociation rate (0.48 s^{-1}) from the (presumably) trailing head was 32-times faster than that of the leading head (0.015 s^{-1}) and a similar mechanism occurs with ADP[10,21]. Inhibition of ADP dissociation from the lead head is thought to be essential for long processive movements. Our results indicate that the main pathway of the MyoV-HMM ATPase is by the central shaded line of intermediates in Fig. 4. The recently detached (formerly rear) head containing ATP or ADP-P_i rapidly swings forward to the leading position where it binds actin (state (1)). On binding to actin, this head quickly releases P_i (state (1) to (2) in Fig. 4)[7]. ADP then

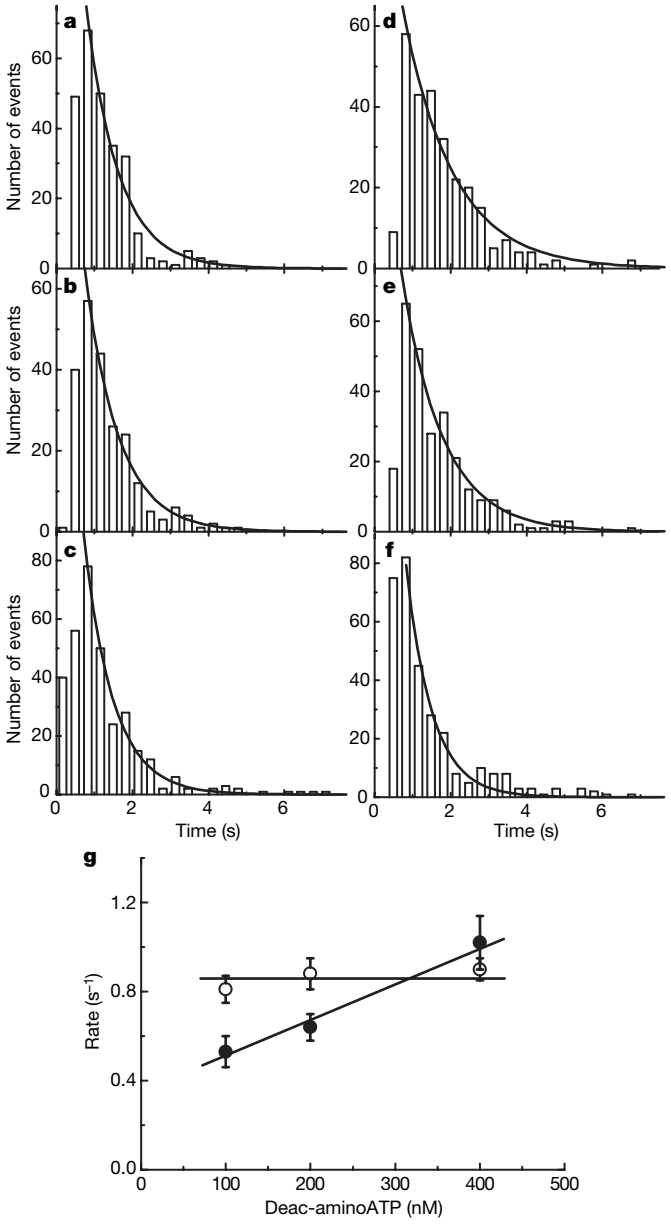

Figure 3 | Histogram of lifetimes of deac-aminonucleotide association and dissociation. **a–c**, Histograms of the lifetimes before deac-aminonucleotide dissociation at 100 nM ($n = 261$ steps, 44 MyoV-HMM molecules), 200 nM ($n = 262$ steps, 38 myosin Va molecule) and 400 nM ($n = 310$ steps, 35 MyoV-HMM molecules) deac-aminoATP. The solid lines represent the exponential fit of the dwell-time distribution. The fitted lifetimes at 100 nM (**a**), 200 nM (**b**), and 400 nM (**c**) deac-aminoATP are 0.85 ± 0.06 s ($r^2 = 0.98$), 0.88 ± 0.07 s ($r^2 = 0.98$) and 0.77 ± 0.04 s ($r^2 = 0.98$; all mean ± s.d.), respectively, corresponding to rate constants of 0.82 ± 0.06 s^{-1}, 0.79 ± 0.07 s^{-1} and 0.90 ± 0.05 s^{-1}. **d–f**, Histograms of the lifetimes of deac-aminoATP binding. The fitted lifetimes at 100 nM ($n = 296$; **d**), 200 nM ($n = 267$; **e**) and 400 nM ($n = 309$; **f**) deac-aminoATP are 1.32 ± 0.17 s ($r^2 = 0.98$), 1.08 ± 0.11 s ($r^2 = 0.98$) and 0.68 ± 0.08 s ($r^2 = 0.98$; all mean ± s.d.), respectively. Note that the number of spots is the same as **a–c**. This corresponds to rate constants of 0.53 ± 0.07 s^{-1}, 0.64 ± 0.06 s^{-1} and 1.02 ± 0.12 s^{-1}, respectively. Statistical analysis (Student's *t*-test) between each experimental point showed that the data of ADP dissociation rate from three conditions are not significantly different ($P(T \leq t) = 0.68$, 0.09 and 0.16 of 100 versus 200, 100 versus 400 and 200 versus 400 nM deac-aminoATP, respectively. In contrast, *P* values of ATP binding rates are significantly different as shown ($P(T \leq t) = 0.01$, 0.028 and 0.02 for 100 versus 200, 100 versus 400 and 200 versus 400 nM deac-aminoATP, respectively). **g**, Concentration dependence of the rates of deac-aminoADP dissociation (open circles) and deac-aminoATP binding (filled circles). The deac-aminoATP binding data were fit by linear regression which gave a slope corresponding to a second order rate constant of 1.67 $\mu M^{-1} s^{-1}$. Note the non-zero intercept which is also present in the solution kinetic measurements of deac-aminoATP binding to acto-HMM in Supplementary Fig. 9. A non-zero intercept is predicted by modelling the kinetic mechanism and is seen in some published studies[5] but is not readily observed because of the large extrapolation from the high nucleotide concentrations typically used in kinetic studies. The horizontal line through the deac-aminoADP dissociation data represents the average of the mean value for the three nucleotide concentrations (0.86 s^{-1}).

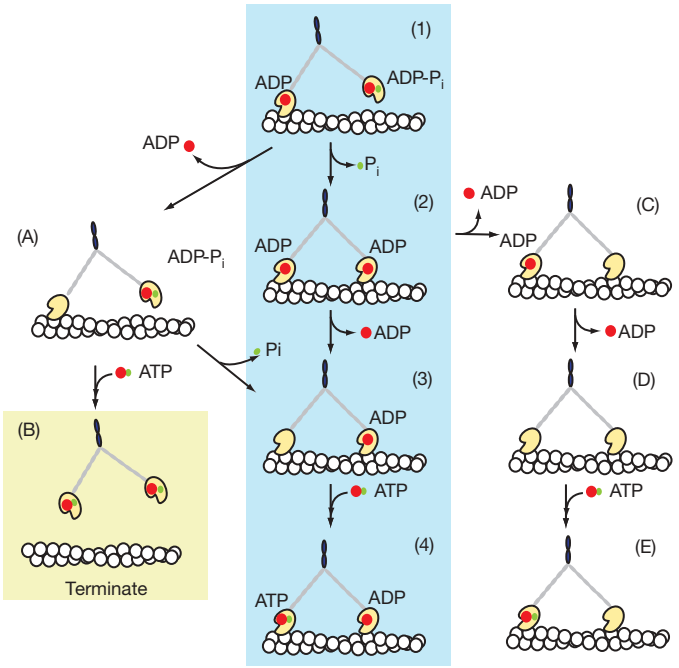

Figure 4 | A scheme of the tight coupling pathway of myosin Va. The mechanism shown by intermediates (1) to (4) is the main pathway of stepping during a MyoV-HMM processive run. Termination of runs would occur by pathway (1) to (A) to (B) or more rarely by (C) to (D) to (E) to (A) to (B). Red spots represent ADP and green spots represent P_i.

dissociates from the trailing head (state (2) to (3)) which allows a new ATP to bind. This results in a rapid detachment of that head, allowing the lead head to undergo its power stroke and repositioning the detached head to become the new lead head (state (3) to (4)). This model accounts for the 36-nm forward steps taken by the Alexa-Fluor-568–MyoV-HMM that occur coincidently with the 18-nm movement and a doubling of the intensity of the nucleotide fluorescence. An 18-nm backward step of nucleotide fluorescence would occur if deac-aminoADP dissociated first from a lead head (state (2) to (C)). We did not observe such steps, which attest to the high level of strain-dependent gating between the kinetics of the two heads of MyoV-HMM. Termination of runs principally occurs by the route (1) to (A) to (B). This is consistent with most termination cases in which the myosin has only one deac-aminonucleotide bound.

Here we have directly observed the substrate binding and product dissociation steps of single motors moving along their tracks. The data show the relationship between these steps and the mechanism of processive movement of myosin Va on actin. These observations directly demonstrate that, as previously proposed, myosin Va is a tightly coupled motor[2,4–11,19]. Each step in a processive run involves the binding of an ATP molecule to the trail head of the myosin Va, which is rapidly followed by a 36-nm step along the actin and subsequently by the dissociation of ADP from the trail head. Deac-aminoATP should be a useful analogue for other single-molecule studies such as combined optical trapping and total internal reflection fluorescence (TIRF) microscopy.

METHODS SUMMARY

Protein purification and labelling. Mouse MyoV-HMM, MyoV-S1 and calmodulin were purified as previously described[22]. Calmodulin was labelled with Alexa Fluor 568 and exchanged for endogenous calmodulins into MyoV-HMM in a similar method to that previously described[3,22].

Data acquisition and analysis. The single molecule *in vitro* motility assay was carried out essentially as previously described[22]. Dual imaging of deac-aminonucleotide and Alexa-Fluor-568-labelled MyoV-HMM were conducted using an Olympus IX81 microscope equipped for two fibre optic input cables using the DualView system[23]. Images were taken at a frame rate of 330 ms and the position of each fluorescent spot was determined using the FIONA method[18].

Transient kinetic data. Measurement of the deac-aminoATP binding and deac-aminoADP dissociation were performed on a KinTek stopped-flow spectrofluorimeter as previously described[10,17].

Full Methods and any associated references are available in the online version of the paper at www.nature.com/nature.

Received 14 March; accepted 3 June 2008.
Published online 30 July 2008.

1. Sellers, J. R. & Weisman, L. S. *Myosins: A Superfamily of Molecular Motors, Proteins and Cell Regulation* Vol. 7 (ed. Coluccio, L) 289–324 (Springer, 2008).
2. Vale, R. D. Myosin V motor proteins: marching stepwise towards a mechanism. *J. Cell Biol.* **163,** 445–450 (2003).
3. Sakamoto, T., Yildiz, A., Selvin, P. R. & Sellers, J. R. Step-size is determined by neck length in myosin V. *Biochemistry* **44,** 16203–16210 (2005).
4. Mehta, A. D. *et al.* Myosin-V is a processive actin-based motor. *Nature* **400,** 590–593 (1999).
5. Rief, M. *et al.* Myosin-V stepping kinetics: a molecular model for processivity. *Proc. Natl Acad. Sci. USA* **97,** 9482–9486 (2000).
6. De La Cruz, E. M., Wells, A. L., Rosenfeld, S. S., Ostap, E. M. & Sweeney, H. L. The kinetic mechanism of myosin V. *Proc. Natl Acad. Sci. USA* **96,** 13726–13731 (1999).
7. Rosenfeld, S. S. & Sweeney, H. L. A model of myosin V processivity. *J. Biol. Chem.* **279,** 40110–40111 (2004).
8. Purcell, T. J., Sweeney, H. L. & Spudich, J. A. A force-dependent state controls the coordination of processive myosin V. *Proc. Natl Acad. Sci. USA* **102,** 13873–13878 (2005).
9. Veigel, C., Schmitz, S., Wang, F. & Sellers, J. R. Load-dependent kinetics of myosin-V can explain its high processivity. *Nature Cell Biol.* **7,** 861–869 (2005).
10. Forgacs, E. *et al.* Kinetics of ADP dissociation from the trail and lead heads of actomyosin V following the power stroke. *J. Biol. Chem.* **283,** 766–773 (2007).
11. Veigel, C., Wang, F., Bartoo, M. L., Sellers, J. R. & Molloy, J. E. The gated gait of the processive molecular motor, myosin V. *Nature Cell Biol.* **4,** 59–65 (2001).
12. Funatsu, T., Harada, Y., Tokunaga, M., Saito, K. & Yanagida, T. Imaging of single fluorescent molecules and individual ATP turnovers by single myosin molecules in aqueous solution. *Nature* **374,** 555–559 (1995).
13. Ishijima, A. *et al.* Multiple- and single-molecule analysis of the actomyosin motor by nanometer piconewton manipulation with a microneedle: Unitary steps and forces. *Biophys. J.* **70,** 383–400 (1996).
14. Tokunaga, M., Kitamura, K., Saito, K., Iwane, A. H. & Yanagida, T. Single molecule imaging of fluorophores and enzymatic reactions achieved by objective-type total internal reflection fluorescence microscopy. *Biochem. Biophys. Res. Commun.* **235,** 47–53 (1997).
15. Oiwa, K. *et al.* Comparative single-molecule and ensemble myosin enzymology: sulfoindocyanine ATP and ADP derivatives. *Biophys. J.* **78,** 3048–3071 (2000).
16. Webb, M. R., Reid, G. P., Munasinghe, V. R. & Corrie, J. E. A series of related nucleotide analogues that aids optimization of fluorescence signals in probing the mechanism of P-loop ATPases, such as actomyosin. *Biochemistry* **43,** 14463–14471 (2004).
17. Forgacs, E. *et al.* Kinetic mechanism of myosinV-S1 using a new fluorescent ATP analogue. *Biochemistry* **45,** 13035–13045 (2006).
18. Yildiz, A. *et al.* Myosin V walks hand-over-hand: single fluorophore imaging with 1.5-nm localization. *Science* **300,** 2061–2065 (2003).
19. Dunn, A. R. & Spudich, J. A. Dynamics of the unbound head during myosin V processive translocation. *Nature Struct. Mol. Biol.* **14,** 246–248 (2007).
20. Burgess, S. *et al.* The prepower stroke conformation of myosin V. *J. Cell Biol.* **159,** 983–991 (2002).
21. Rosenfeld, S. S., Houdusse, A. & Sweeney, H. L. Magnesium regulates ADP dissociation from myosin V. *J. Biol. Chem.* **280,** 6072–6079 (2005).
22. Sakamoto, T. *et al.* Neck length and processivity of myosin V. *J. Biol. Chem.* **278,** 29201–29207 (2003).
23. Thirumurugan, K., Sakamoto, T., Hammer, J. A. III, Sellers, J. R. & Knight, P. J. The cargo-binding domain regulates structure and activity of myosin 5. *Nature* **442,** 212–215 (2006).
24. Wang, F. *et al.* Effect of ADP and ionic strength on the kinetic and motile properties of recombinant mouse myosin V. *J. Biol. Chem.* **275,** 4329–4335 (2000).
25. Webb, M. R. & Corrie, J. E. Fluorescent coumarin-labeled nucleotides to measure ADP release from actomyosin. *Biophys. J.* **81,** 1562–1569 (2001).
26. Sakamoto, T., Amitani, I., Yokota, E. & Ando, T. Direct observation of processive movement by individual myosin V molecules. *Biochem. Biophys. Res. Commun.* **272,** 586–590 (2000).
27. Thompson, R. E., Larson, D. R. & Webb, W. W. Precise nanometer localization analysis for individual fluorescent probes. *Biophys. J.* **82,** 2775–2783 (2002).

Supplementary Information is linked to the online version of the paper at www.nature.com/nature.

Acknowledgements We thank F. Zhang, A. Smith and G. Reid for technical assistance; E. Yokoi for the TIRF illuminator to combine two optical cables; C. Fanghella for technical help in the calculation of the number of photons; and C. Weaver for help with Metamorph. We are appreciative of the critical comments on the manuscript made by P. J. Knight and E. Homsher. M.R.W. was supported by

the Medical Research Council, UK. J.R.S. and T.S. were supported by the National Heart, Lung and Blood Intramural Program. H.D.W. and E.F. were supported by NIH EB00209 and a postdoctoral fellowship from the American Heart Association.

Author Contributions Single molecule motility experiments and data analysis were performed by T.S. and kinetic experiments data by E.F. Deac-aminoATP/ADP were provided by M.R.W. T.S., J.R.S. and H.D.W. participated in the conception of the experiment. T.S. wrote the first draft of the manuscript and all authors participated in producing the final version. All authors participated in discussion and interpretation of the data.

Author Information Reprints and permissions information is available at www.nature.com/reprints. Correspondence and requests for materials should be addressed to J.R.S. (Sellersj@mail.nih.gov).

METHODS

Preparation of proteins. Mouse MyoV-HMM and MyoV-S1 were purified from Sf9 cells after infection with baculoviruses driving the expression of the HMM (or S1) and calmodulin[24]. Calmodulin was purified from bovine testes and labelled with Alexa Fluor 568 succimidyl ester (Invitrogen)[22]. The molar ratio of Alexa Fluor 568 per calmodulin was determined to be 1.8 from the absorbance in solution and a molar extinction coefficient of 91,300 $M^{-1}\,cm^{-1}$ for Alexa Fluor 568 and $\varepsilon^{0.1\%} = 0.18$ at 280 nm for calmodulin. The labelled calmodulin (molar ratio of 20 per MyoV-HMM) was exchanged with endogenous calmodulin as previously described[22]. This resulted in an average of six Alexa Fluor 568 dyes per MyoV-HMM, as determined spectrophotometrically. This value was confirmed by comparing the intensity of single Alexa Fluor 568 molecules bound nonspecifically to a surface (2,000 a.u.) with that of the average intensity of Alexa-Fluor-568–MyoV-HMM (12,000 a.u.). Biotinylated actin and biotinylated BSA were prepared[22] and deac-aminoATP and deac-aminoADP were synthesized as described previously[25].

Emission and excitation spectra of 0.5 μM deac-aminoADP in the presence and absence of 1 μM MyoV-HMM were taken with a Fluoromax-3 spectrofluorimeter (HORIBA Jobin Yvon, NJ) using 2 nm slits.

Two-line total internal reflection fluorescence microscopy. Alexa-Fluor-568-labelled MyoV-HMM and deac-aminoATP were observed by objective-type TIRF microscopy using an Olympus IX81 microscope and a ×60, 1.45 numerical aperture PlanApo objective lens with two magnifying (relay) lenses (×1.6 in the microscope and ×2.5 in front of the camera). The temperature was kept at 25 °C with an environmental box (Precision plastics). To visualize two colours of fluorescence simultaneously, we used the 568 nm line from an Ar-Kr Laser (model I70C, Spectra physics) for Alexa Fluor 568 and the 442 nm line from a He-Cd Laser (model IK41711-G, KIMMON) for deac-aminoATP. Both laser lines were combined by an acousto-optical tunable filter (Prairie Technologies), which also controlled the laser power. After the acousto-optical tunable filter, the two laser lines were separated by a dichroic mirror onto optical fibres. This allows both wavelengths to be in focus at the same time. The two fibres are guided to individual TIRF illuminators located at the rear end of the microscope. Illumination at 442 nm was by the Olympus TIRF apparatus and the illumination at 568 nm was by the position usually occupied by the mercury arc lamp housing. The two laser lines from the two illuminators were combined with a dichroic mirror and introduced into the objective lens. The power of both the 442 nm and 568 nm beams was 10 mW to 20 mW in front of the objective lenses. The emitted light was passed through a dual line dichroic mirror (442/568, Chroma) and split by a dichroic mirror (552dcr, Chroma) in the Dual-View system (Optical Insights). Fluorescence was detected by an EMCCD camera (DV897, 512BV, Andor technology), at −90 °C with a gain of either 400 or 1,000. Images were digitized by using Metamorph (MSD/Molecular Device ver.7.1).

Intensity measurement of deac-aminoADP bound either to the surface or to MyoV-HMM. To test whether the fluorescence of deac-aminoADP increased in intensity upon binding to MyoV-HMM in the microscope, we directly observed single molecules of deac-aminoADP in the presence and absence of MyoV-HMM. First, 10 pM deac-aminoADP was added into a flowcell coated with 0.1% nitrocellulose and incubated for 2 min at room temperature. Free deac-aminoADP was washed out using motility assay buffer (40 mM KCl, 20 mM MOPS, 4 mM $MgCl_2$, 0.1 mM EGTA, 1 μM calmodulin, and 50 mM DTT, pH 7.5, 25 °C). The solutions also included an oxygen scavenging system composed of 25 μg ml^{-1} glucose oxidase, 45 μg ml^{-1} catalase and 2.5 mg ml^{-1} glucose. Deac-aminoADP was imaged at 442 nm using the TIRF microscopy set up described above at EMCCD camera gains of 1,000 (Fig. 1a, e) and 400 (Fig. 1b, f); images were acquired in 330 ms windows. On a second slide, 10 pM MyoV-HMM was added into the flowcell and incubated for 2 min at room temperature. Free MyoV-HMM was washed out using motility assay buffer. Deac-aminoADP (10 nM) was added into the flowcell and the sample was imaged at 442 nm and 568 nm at the same two camera gains. Under these conditions at the single-molecule level in the microscope, the intensity of deac-aminoADP increased 4 fold upon binding to MyoV-HMM compared to the 25 fold change in solution.

Single-molecule motility assay and data analysis. Single-molecule motility assays were performed as previously described[26]. Position data for Alexa-Fluor-568–MyoV-HMM and deac-aminoATP were analysed by FIONA[18]. The integrated intensities of 15 × 15 pixel areas were measured at the indicated concentrations using Metamorph. To observe single-molecule movements of MyoV-HMM and deac-aminoATP simultaneously, we changed the concentration of Alexa-Fluor-568–MyoV-HMM to reduce background. At 100 nM and 200 nM deac-aminoATP concentrations, 200 pM Alexa-Fluor-568–MyoV-HMM was used, whereas at 400 nM deac-aminoATP, 4 pM Alexa-Fluor-568–MyoV-HMM was used. Steps were identified by eye and marked by hand.

Run lengths of Alexa-Fluor-568–MyoV-HMM were measured with either 1 mM ATP or 1 mM deac-aminoATP. Actin filaments were labelled with 10% Alexa-Fluor-488-phalloidin and 90% phalloidin. The determination of run length was performed as described previously[22], except that only myosin molecules that dissociated before reaching the end of actin filaments were scored. The average length of an actin filament was 12.5 μm. Velocities with various deac-aminoATP concentrations were measured by time lapse in which data were taken at 10 s intervals with a 300 ms exposure time. Sequential images were taken to analyse velocity.

Determination of number of photons. We determined the number of photons from the integrated intensity of a 10 × 10 pixel image of each chosen spot. Deac-aminoADP was bound nonspecifically to the surface or to MyoV-HMM, which was bound on a nitrocellulose-coated surface. The estimated total number of photons in the spot at various camera gains was calculated as previously described[27]. Alternatively, the number of photons, n, was calculated using an equation $n = 60.14\ I/a$ provided by Andor Technology (data not shown) in which 60.14 is the camera sensitivity at 10 MHz, electron multiplying amplifier, ×1.0 preamp setting (electron per A/D count), a is the percentage of quantum efficiency of the camera at the appropriate wavelength, and I is the detected integrated intensity. Results obtained by the two methods gave reasonable agreement. At least 10,000 photons are required to obtain 2.5 nm localization[19]. Determination of localization accuracy from single-molecule fluorophores has been calculated by theoretical equations[27] and measured experimentally[18].